Materials Today Sustainability 26 (2024) 100701

Contents lists available at ScienceDirect

Materials Today Sustainability

journal homepage: www.journals.elsevier.com/materials-today-sustainability

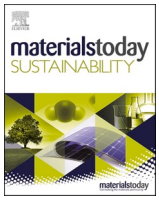

An effective material for solar steam generation applications: Gradient graphene sponge

Elif Erçarıkcı [a], Ezgi Topçu [a], Züleyha Kudaş [a], Zeriş Aksu [a], Murat Alanyalıoğlu [b], Kader Dağcı Kıranşan [a,*]

[a] Department of Chemistry, Science Faculty, Atatürk University, Erzurum, 25240, Turkey
[b] Department of Food Processing, Vocational School, Bilecik Şeyh Edebali University, Bilecik, 11230, Turkey

ARTICLE INFO

Keywords:
Graphene sponge material
Gradient structure
Solar energy
Clean water

ABSTRACT

The efficient use of solar energy for clean water is a renewable and environmentally-friendly route to solve global water scarcity. For this, we report the preparation of light, mechanically durable, and effective photothermal material. A simple acid impregnation method was applied to graphene sponge material (GSM) possessing hydrophobic character to gain partial hydrophilicity to obtain a gradient structure. The morphological and structural properties of the gradient graphene sponge material (GGSM) were carried out using scanning electron microscopy, X-ray photoelectron spectroscopy, Raman spectroscopy, X-ray powder diffraction patterns, Fourier-transformed infrared spectroscopy, and water drop contact angle measurements. GGSM showed fast and effective water vapor conversion performance due to the gradient structure, as well as the high rate of sunlight absorption and photothermal conversion thanks to graphene. With the advantageous feature of gradient structure, GGSM achieved a high water vapor conversion capacity (1.79 kg/m^{2}h) and solar thermal efficiency of 57% compared to GSM (1.58 kg/m^{2}h; 45%). This new material provides a novel approach to solar energy applications.

1. Introduction

Graphene, a monolayer of carbon atoms tightly packed in a two-dimensional crystal, has attracted more and more interest due to its unique chemical structure and physical properties [1,2]. Recent studies have demonstrated that graphene nanosheets can be easily fabricated in large quantities from commercial graphite. Free-standing flexible 2-dimensional (2D) graphene papers [3] and 3D graphene sponges [4] can be simply produced from the graphene nanosheets. 3D graphene sponges are being actively explored in applications such as supercapacitors [5], lithium-ion batteries [6], membranes [7], sensors [8], and solar steam generators [9] (SSG). The expectation from the materials used in SSG is that it provides clean water with high efficiency and low cost from direct natural sunlight [10]. The focus for this purpose is to develop materials with both cost-effective and easy scalabilities that can efficiently absorb sunlight and convert it into thermal energy [11]. Recently, metallic nanoparticles such as gold [12,13] and alumina [14] have been frequently investigated for clean water production in SSG, but their possible practical applications are limited due to their high cost, complex manufacturing processes, and potential safety issues [12]. At this point, 3D graphene sponges with high sunlight absorption and thermal insulation appear as an effective candidate for the photothermal conversion mechanism [15–17].

For efficient steam production, graphene sponges should have a good water transmission performance, in addition to high solar absorption and photothermal conversion [18,19]. Several methods to prepare 3D graphene sponges have been explored quite extensively. Among those, the chemical vapor deposition method has the advantage of producing solar vapor efficiently, however, the difficult preparation conditions may prevent their wide use in practical applications [11,20]. For the hydrothermal synthesis method, it can be a problem to obtain large-area material since the size of the prepared material is limited by the size of the hydrothermal vessel. In the foaming-drying method, it is possible to fabricate the material in the desired size, unfortunately, graphene sponges gain a highly hydrophobic structure after the thermal heating process. The increase in the hydrophobic property also negatively affects the thermal insulation and the capillarity that enables the water to be transmitted to the surface [15,19]. The synthesis of graphene sponges with a gradient structure (from hydrophobic to hydrophilic) can be considered in order to partially eliminate the hydrophobic character and

* Corresponding author.
E-mail address: kdagci@atauni.edu.tr (K. Dağcı Kıranşan).

https://doi.org/10.1016/j.mtsust.2024.100701
Received 14 December 2023; Received in revised form 19 January 2024; Accepted 1 February 2024
Available online 20 February 2024

increase the water transport performance of materials prepared through simple foaming-drying. Thus, both an effective photothermal transformation and a high water transmission capacity can be achieved through graphene sponges with a gradient structure.

Until now, enormous effort has been made to increase the performance of graphene-based materials in SSG. For example, Ran Niu et al. prepared MnO_2-modified carbon fabric whose evaporation rate can reach 2.67 kg m^{-2} h^{-1} with a solar-thermal conversion efficiency of 89.5 % [21]. Ning Liu et al. developed a Janus-structured natural wood with a porous carbon-modified surface. Under solar illumination intensity, this material showed an evaporation rate of 2.38 kg m^{-2} h^{-1} [22]. Zifen Fan et al. reported a MnO/C material prepared by natural pyrolysis of Mn-MOF which shows a 2.38 kg m^{-2} h^{-1} steam generation performance [23]. The materials in these studies have a Janus structure and very complex techniques are used for the preparation. Besides, graphene-based materials are widely used in SSG systems. For example, Li et al. prepared a graphene-based Janus structure by placing a GO film on 2D polystyrene foam wrapped with hydrophilic cellulose, and this material showed an evaporation rate of 1.45 kg m^{-2} h^{-1} [19]. Ghasemi et al. reported carbon foam with an exfoliated graphite-modified surface showing 1.21 kg m^{-2} h^{-1} evaporation rate [24]. Li et al. developed a material by using the CNT/GO ink on a three-dimensional printer whose evaporation rate reaches 1.25 kg m^{-2} h^{-1} [16]. In all these and similar studies, in order to achieve high efficiency, almost all designs are costly and require complex multi-component systems, including extra support or insulation material, therefore, both the scalability and feasibility of these methods are limited [25]. We report the development of a new approach and corresponding single material structure (non-Janus) that localizes the solar energy where evaporation occurs and minimizes the heat losses leading to enhanced solar thermal efficiency at low optical concentration while generating steam.

Herein, we successfully prepared a 3D graphene sponge material (GSM) possessing hydrophobic character using a simple and low-cost foaming-drying method and then brought it into a hydrophilic-hydrophobic gradient structure by a simple acid impregnation method. In this gradient graphene sponge material (GGSM), while the gradient structure provides a fast and effective water transport performance, a 3D graphene architecture maintains a high rate of sunlight absorption and photothermal transformation. Compared with GSM, GGSM showed a higher water vapor conversion and steam evaporation efficiency owing to the gradient (hydrophilic-hydrophobic) structure. This study opens a new possibility to develop highly efficient 3D graphene-based material for the generation of pure water.

2. Experimental

2.1. Synthesis of GO

Graphene oxide (GO) was prepared according to our previous study [26–28]. A certain amount of GO powder was subjected to sonication in distilled water for 1 h to obtain a dispersion of GO nanosheets with a concentration of 7.0 mg/mL.

2.2. Preparation of GSM

GSM was prepared using a foaming-drying method. Briefly, 20 mL of GO aqueous dispersion containing ascorbic acid (AA, 400 mg) as a reductant was vigorously stirred after the addition of sodium dodecyl sulfate (SDS) (50% by weight) for foaming. The resulting foamy dispersion was treated at 75 °C for 1 h and the graphene hydrogel sponge (GHS) was obtained. GHS was frozen at −18 °C for about 5 h and then cooled naturally to room temperature. Subsequently, the as-prepared GHS was dried at 90 °C, then washed several times with ethanol and deionized water to remove excess AA. Finally, free-standing GSM was fabricated by annealing GHS at 350 °C (Fig. 1) [17,29].

2.3. Preparation of GGSM

GGSM was prepared using a simple acid impregnation method. GSM at the height of 1.2 cm was immersed in a cylindrical glass vessel containing about 2 mm of different acid solutions. While GSM was gradually impregnated with the acid, the acid oxidized the graphene structure of GSM according to the acid-treatment time. Regions of GSM that interact more with the acid solution, undergo more oxidation, resulting in a gradient structure of GSM (GGSM). The structural properties of the prepared GGSM samples were characterized as three different regions. The region directly immersed in acid was called GGSM-R1 (between 0 and 4 mm GSM height), and the region that had no interaction with acid was called GGSM-R3 (between 8 and 12 mm GSM height). The region in the middle of the lower and upper parts was named as GGSM-R2 (between 4 and 8 mm GSM height) (Fig. 2). After the acid impregnation process, GGSM was washed several times to remove the excess acid and then dried at room temperature (fig. S1).

2.4. Characterization

The morphologies of the GSM and GGSM samples were investigated by a ZEISS SIGMA 300 field-emission scanning electron microscope (FESEM) equipped for elemental analysis by EDX. The structures and compositions of the as-prepared materials were characterized by X-ray powder diffraction (XRD) using a Rigaku Mini Flex X-ray diffractometer with Cu Kα radiation (λ = 1.5406 Å). X-ray photoelectron spectroscopy (XPS) measurements of GSM and GGSM were performed on a Spect-Flex spectrometer with monochromatic Al Kα (1486.71 eV) X-ray radiation. The Raman spectra of GSM and GGSM was recorded on a WITech alpha 300R micro-Raman spectrometer, with an excitation laser wavelength of 532 nm. N_2 adsorption−desorption isotherm was measured at 77 K on an Auto Sorb iQ-C TCD analyzer and used to calculate the specific surface area through Brunauer−Emmett−Teller (BET) method. The electrical properties of the materials were measured through resistance measurement by a four-point probe meter (SX1944, Cryogenic Limited PPMS). A contact angle meter (Attention Theta Flex) was used to analyze the hydrophilic-hydrophobic character of GGSM.

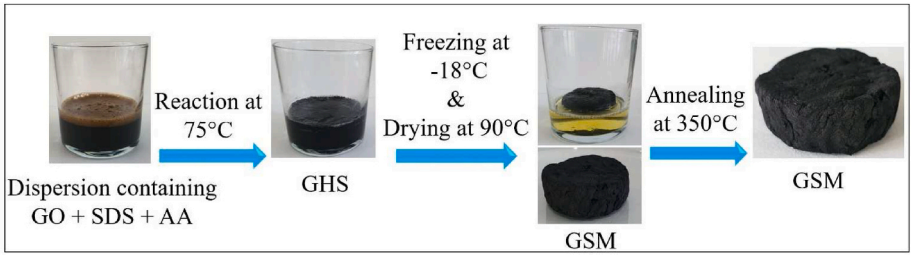

Fig. 1. The preparation procedure of GSM.

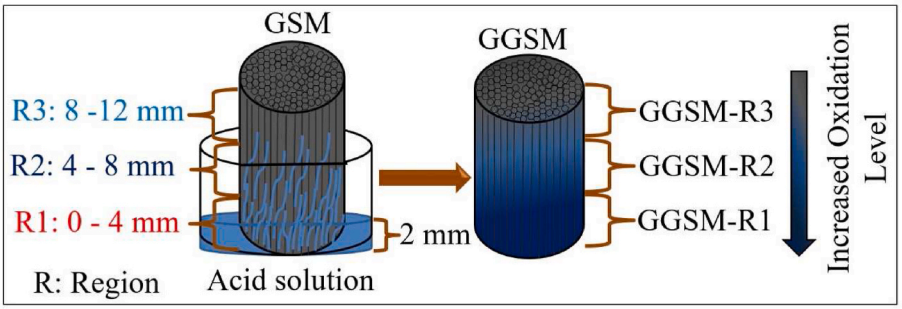

Fig. 2. Conversion procedure of GSM to GGSM.

3. Results and discussion

3.1. The optimization of preparation parameters of GSM

In this work, we adopted a foaming-drying method to fabricate the free-standing GSM for an efficient material in solar steam generators. Firstly, GSMs were fabricated with different amounts (5, 6, 7, 8 mg/mL) of GO dispersions in order to optimize the GO concentration for the preparation of GSM. Photographs of these GSMs in a container filled with water at different times, keeping the AA amount (GO/AA:1/3), thermal treatment time (3 h), and annealing time (4 h) constant are shown in fig. S2. After the treatment with water for 30 min, GSMs prepared using 5 and 6 mg/mL GO dispersions disintegrated, on the other hand, GSMs prepared using 7 and 8 mg/mL GO concentrations displayed high durability to water with no deterioration in sponge structure. In FESEM images of these GSMs in fig. S3, the sponge structure with regular pores was formed in the GSM prepared with 7 mg/mL GO dispersion while for the others, the porous sponge structure deteriorated by stacking GO layers on top of each other (fig. S3). These results showed that 7 mg/mL GO should be used for the preparation of the most water-durable sponge. The second parameter to be optimized is the amount of AA for the reduction of GO. For this, the durability of GSMs prepared with different GO/AA ratios (1:1, 1:2, 1:3, 1:4, and 1:5) were tested against water. From the photographs (fig. S4) and FESEM images (fig. S5), GSM prepared with the GO/AA ratio of 1:3 demonstrated a durable sponge structure with a stable floating in the water. A regular pore structure was not formed in the sponge, since the amount of AA in the ratio of GO/AA = 1:1 and 1:2 was not sufficient to reduce GO, and, the excessive amount of AA led to the formation of a fragile sponge with thick layers (fig. S5). Thus, the optimum GO/AA mass ratio was optimized as 1:3.

Another parameter affecting the mechanical and structural properties of the prepared GSM is the thermal processing time at 90 °C. GSMs prepared from GHSs dried at different times (1, 2, 3, 4, and 5 h) were tested for water stability. In figure S1, 2 and 6 h of thermal treatment were not sufficient to prepare water-durable GSMs, and these prepared materials sank even after a very short period of time. The FESEM image in fig. S7 also showed a regular and porous sponge structure after 3 h of thermal treatment. After 5 h an undesirable layered morphology was formed due to excessive heat treatment. Thus, FESEM images confirmed that the optimum thermal treatment time should be 3 h. Finally, the annealing time was optimized to further increase the mechanical strength of the GSMs. When the stability of the GSMs obtained after annealing at 350 °C for different times (1, 2, 3, 4, and 5 h) is evaluated, the prepared sponge has a highly durable and hydrophobic character since the sufficient reduction is achieved after 3 and 4 h of annealing. The photographs in fig. S8 and FESEM images in fig. S9 showed that the optimized annealing time should be 3 h for a highly durable and stable sponge material. Thus, GSM with high water durability and regular pore size was performed at these optimum conditions for all studies: 7 mg/mL GO dispersion, GO/AA = 1:3 ratios, 3 h thermal treatment time at 90 °C, and 3 h annealing at 350 °C.

The digital photograph in Fig. 3 a showed that GSM prepared under optimum conditions is light enough to be carried by a delicate flower. In addition, there was no change in the shape of GSM after applying a pressure of 100 g. This process was repeated 100 times in succession and the photographs after the cycles demonstrated that GSM has high resistance to mechanical stress and flexibility (Fig. 3b and c).

In fig. S10, the water durability of optimum GSM was tested by keeping it in water for 7 days. It remained quite stable for up to 4 days, however, after the 4th day it started to submerge due to the effect of wetness. Moreover, how much water the GSM absorbs over time was evaluated by measuring the increase in weight. From the weights of GSM in table S1, it was determined that while the increase in weight was quite low until the 4th day after then the weight gain accelerated with the onset of wetting. These results displayed that GSM is resistant to wetting almost %10 for up to 4 days.

3.2. The optimization of preparation parameters of GGSM

The parameters that need to be optimized in the preparation of GGSMs are the activities of the acids used for oxidation, the mixing ratios of the acids, and the duration of the acid treatment [11,20,30,31]. XRD spectroscopy and contact angle measurements were performed to optimize these three parameters. XRD spectra of GGSM-R1, GGSM-R2, and GGSM-R3 prepared by impregnating with HNO_3 and H_2SO_4 were presented in Fig. 4a and b, respectively. After treatment of GSM with HNO_3, the characteristic diffraction peak indexing to the (002) plane of graphene or reduced graphene oxide (rGO) was observed in the XRD pattern for all regions (GGSM-R1, GGSM-R2, and GGSM-R3) of GSM (Fig. 4a). On the other hand, the diffraction peaks of the graphene (at 24.5°) and GO (at 10.9°) appeared only at GGSM-R1, indicating that only the region in contact with the acid was oxidized and a clear gradient oxidation structure is not obtained. XRD pattern in Fig. 4 b showed the diffraction peak of GO for GGSM-R1 and GGSM-R2, besides a typical peak of graphene. In addition, the diffraction peak of graphene (002) shifted to lower 2θ values for GGSM-R2 and GGSM-R1 in Fig. 4 b, indicating that as the graphene oxidized, the distance between the layers (d) increased according to the Bragg equation ($n\lambda = 2\ d \sin\theta$) [32]. Fig. 4c and d showed that GGSM-R3 has a high contact angle of about 140° and exhibits hydrophobic character after treatment with HNO_3 and H_2SO_4 due to not being oxidized. GGSM-R2 showed approximately the same contact angle after two acid treatments, while the contact angle of GGSM-R1 treated with H_2SO_4 (53°) is lower, therefore, GSM demonstrated a better gradient structure with H_2SO_4. Thus, it was concluded that the desired gradient structure was obtained with more successful oxidation by using H_2SO_4.

For GSM with a gradient hydrophilic structure, we thought that better results can be obtained if acid solutions prepared with both H_2SO_4 and HNO_3 are used instead of a single acid. For this purpose, XRD and the measurement of contact angle were performed for the oxidation of GSM with different volume ratios of two acids (H_2SO_4/HNO_3 = 1/2,

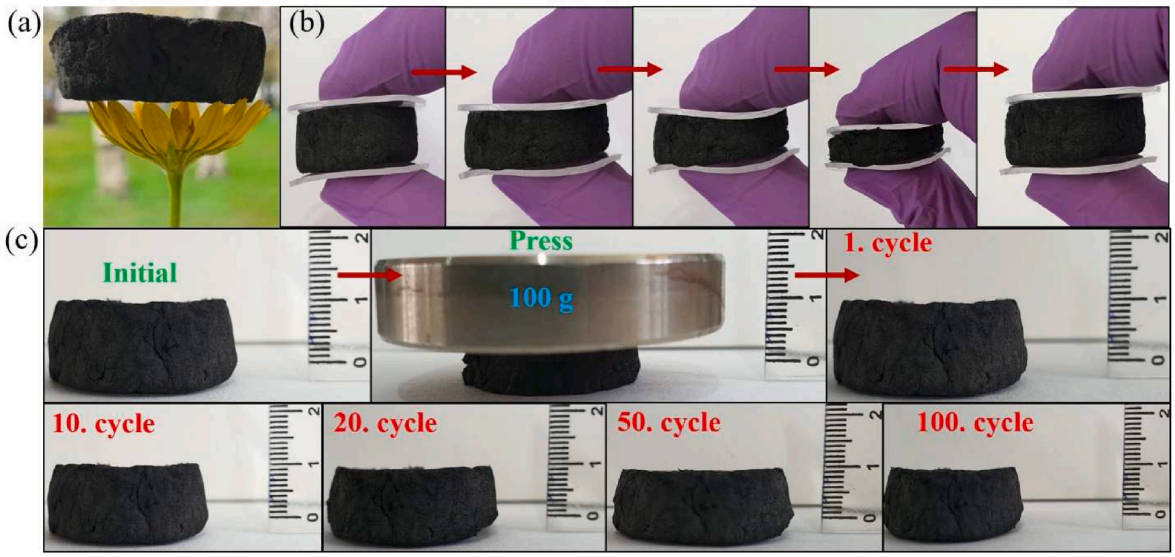

Fig. 3. The digital photographs of lightweight (a) and mechanically flexible (b) GSM. (c) The digital photographs of GSM which is flexible enough to carry a 100g load unchanging its shape for 1 to 100 cycles.

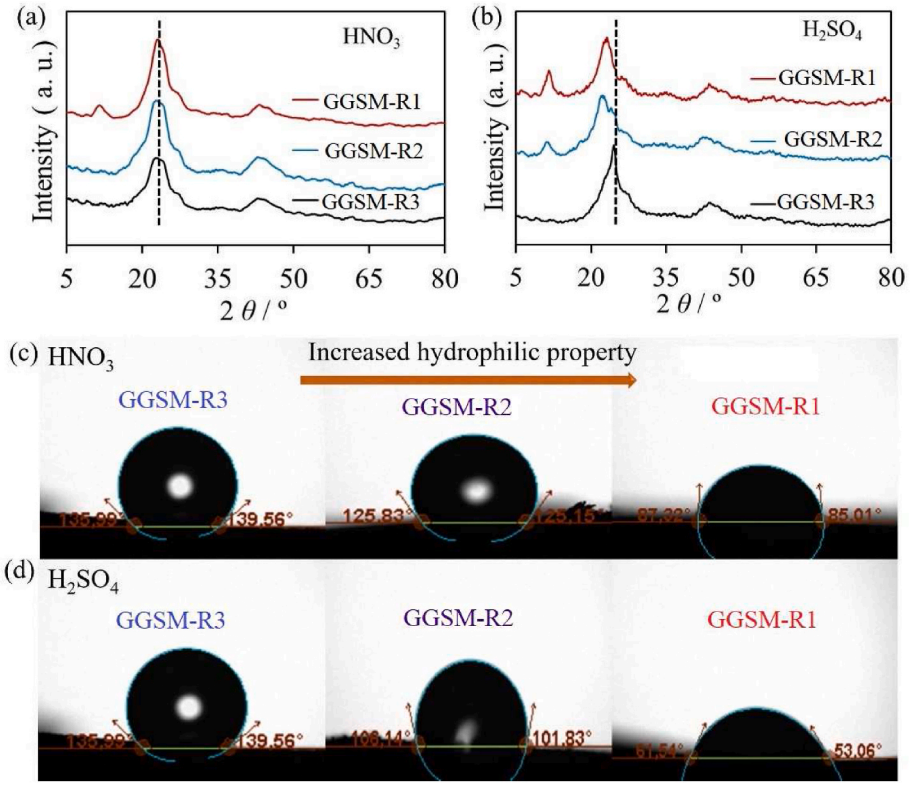

Fig. 4. XRD spectra of GSM after treatment with (a) HNO_3 and (b) H_2SO_4. Water contact angle measurements of GSM after treatment with (c) HNO_3 and (d) H_2SO_4.

$H_2SO_4/HNO_3 = 1$, and $H_2SO_4/HNO_3 = 2$) in Fig. 5. The shift of (002) diffraction of graphene to lower 2θ values (in Fig. 5b) and the difference in contact angle in each region of GSM (in Fig. 5e) demonstrated that GSM with the best gradient structure was obtained after treatment with an acid solution of $H_2SO_4/HNO_3 = 1$ ratio.

Finally, to optimize the acid solution treatment time for the preparation of GGSM, the hydrophobic structure was oxidized by impregnating GSM in an acid mixture ($H_2SO_4/HNO_3 = 1$) for different times (1, 5, 10, and 15 min). The measurement of the contact angle and XRD of the regions of GSM are presented in Fig. 5. For the gradient structure analysis of GSM, the diffraction peak of the GO at 10.9° formed due to the oxidation of graphene (Fig. 6a, b, c, and d) were evaluated. After 1 min of treatment of acid, a diffraction peak of GO was observed only for GGSM-R1 that is in direct contact with the acid (Fig. 6a). The GO peak occurred in GGSM-R1 at a high rate and partially in GGSM-R2 after the acid impregnation of 5 and 10 min (Fig. 6b and c). At the end of 15 min, the entire GSM was oxidized and the diffraction peak of the oxide structure was formed for each region (Fig. 6d). For further evaluation, the measurements of the contact angle of GSM after different impregnation times are presented in Fig. 6e-h. After 5 and 10 min of treatment

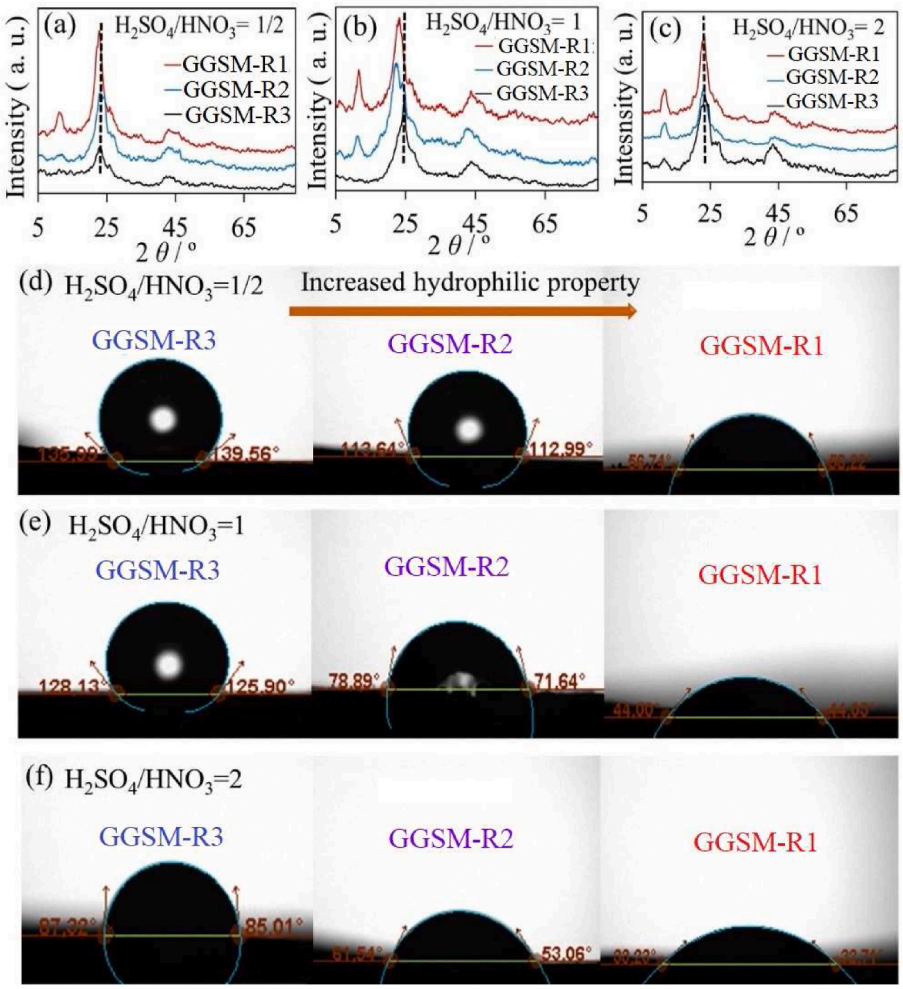

Fig. 5. XRD spectra of GSM treated with H_2SO_4/HNO_3 solution with a volume ratio of (a) 1/2, (b) 1 and (c) 2. The water contact angle measurements of GSM treated with H_2SO_4/HNO_3 solution with a volume ratio of (d) 1/2, (e) 1, and (f) 2.

with the acid, the contact angle values of 125° for GGSM-R3; 94°, 78° and 78°, 61° for GGSM-R2 and GGSM-R1, respectively, were determined, indicating good oxidation for GGSM-R1 and GGSM-R2 (Fig. 6f and g). These results showed that a gradient structure was formed after acid treatment for both 5 and 10 min, thus, the treatment with the acid solution for a minimum of 5 min would be sufficient. The GSM used in subsequent studies was prepared under these optimum conditions and named as gradient GSM (GGSM).

3.3. Characterization of GSM and GGSM

FESEM images in Fig. 7a-i shows the morphology of the three regions of GGSM (GGSM-R1, GGSM-R2, and GGSM-R3). While the FESEM images of GGSM-R3 exhibit a regular 3D sponge structure (Fig. 7 a, b, c), images for GGSM-R2 show a partial deterioration of the structure due to the oxidation increment. For GGSM-R1, excessive oxidation caused collapses in the 3D structure of graphene (Fig. 7 g, h, i).

EDX analysis of GSM and GGSM is presented in fig. S11. Only the C and O atoms was observed in the spectra of GSM and GGSM. While GSM consists of 83% C and 17% O atoms (figure S11a) in GGSM, the percentage of atoms changed along the gradient structure (figure S11b). The atomic ratio of oxygen increased depending on the increase in the degree of oxidation (hydrophilic property) (inset of figure S11b), confirming the gradient structure of GGSM.

3.4. Structural characterization

XRD spectra of three different regions of GGSM are presented in Fig. 8. In the XRD spectrum of all regions of the GGSM in Fig. 8 a, the characteristic diffraction peak of graphene was observed at 24.6°. An additional peak was determined at 10.6° in GGSM-R2 and GGSM-R1, which corresponds to GO due to oxidation. The intensity of the GO peak formed in GGSM-R1 is higher than that of in GGSM-R2 [8]. XRD results suggested that the gradient structure was successfully formed in GGSM.

The Raman spectra of three different parts of the GGSM are shown in Fig. 8 b. The Raman spectrum of all parts showed two prominent peaks at 1360 and 1597 cm^{-1}, corresponding to the well-documented D and G bands, respectively. The I_D/I_G ratios for GGSM-R1, GGSM-R2, and GGSM-R3 were determined as 1.25, 1.17, and 1.09, respectively. The highest I_D/I_G ratio for GGSM-R1 is an expected result since the increase in the hydrophilic character in the graphene sponge is due to the increment of oxidation. Similarly, lower I_D/I_G ratios were observed due to the decrease in oxidation for GGSM-R2 and GGSM-R3.

XPS was employed to measure elemental composition on the surface of the GGSM. Fig. 8 c showed the survey spectra of GGSM-R1, GGSM-R2, and GGSM-R3. From GGSM-R1 to GGSM-R3, the intensity of the C peak increased while that of O decreased dramatically, indicating the formed gradient structure in GGSM.

Deconvoluted XPS spectra of the GSM and GGSM were presented in fig. S12. Both the C1s XPS spectrum of GSM and GGSM displayed the

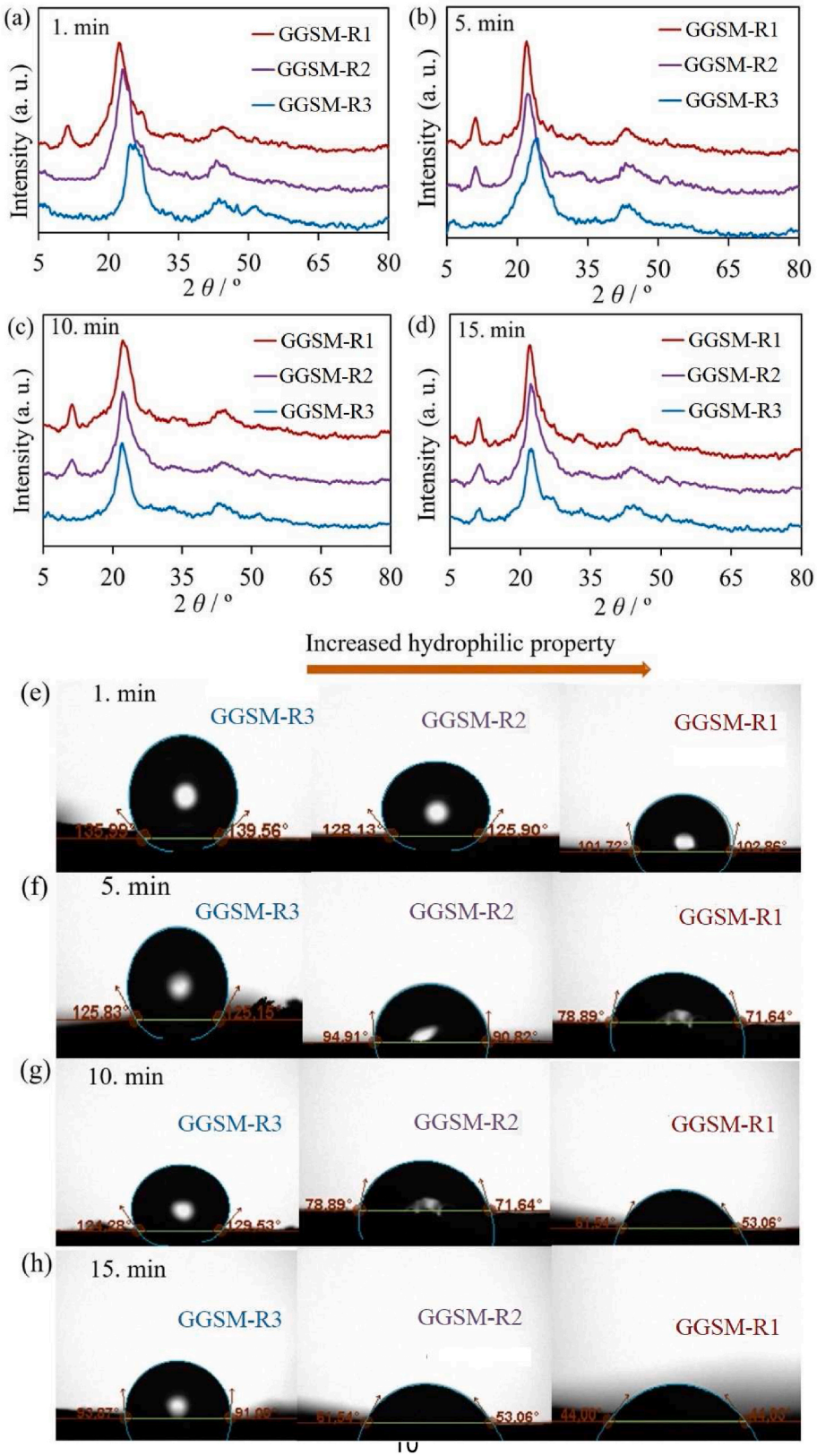

Fig. 6. XRD spectra and water contact angle measurement of GGSM-R1, GGSM-R2, and GGSM-R3 after treatment with an acid mixture at a ratio of $H_2SO_4/HNO_3 = 1$ for (a), (e) 1 min; (b), (f) 5 min; (c), (g) 10 min; and (d), (h) 15 min.

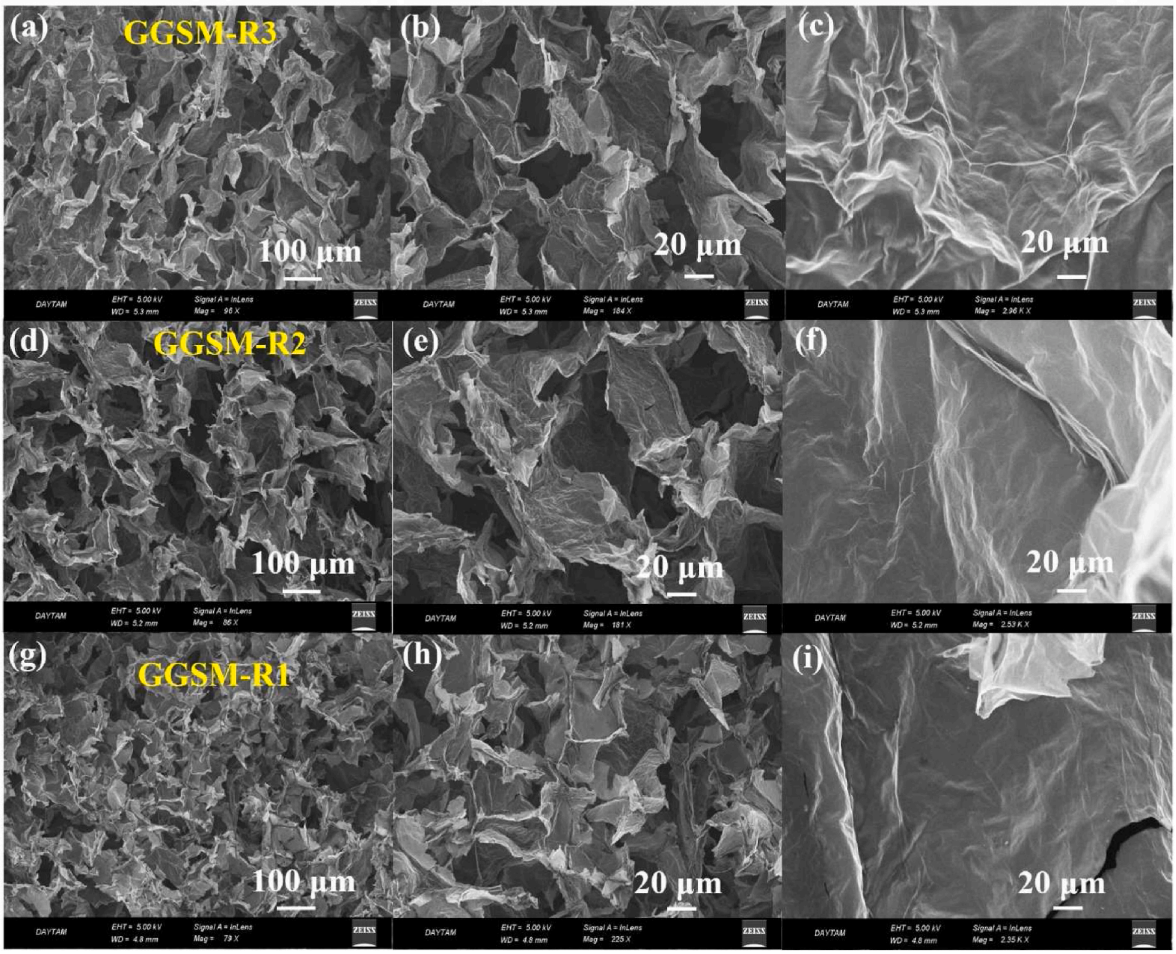

Fig. 7. FESEM images of (a, b, c) GGSM-R3, (d, e, f) GGSM-R2, and (g, h, i) GGSM-R1 at different magnifications.

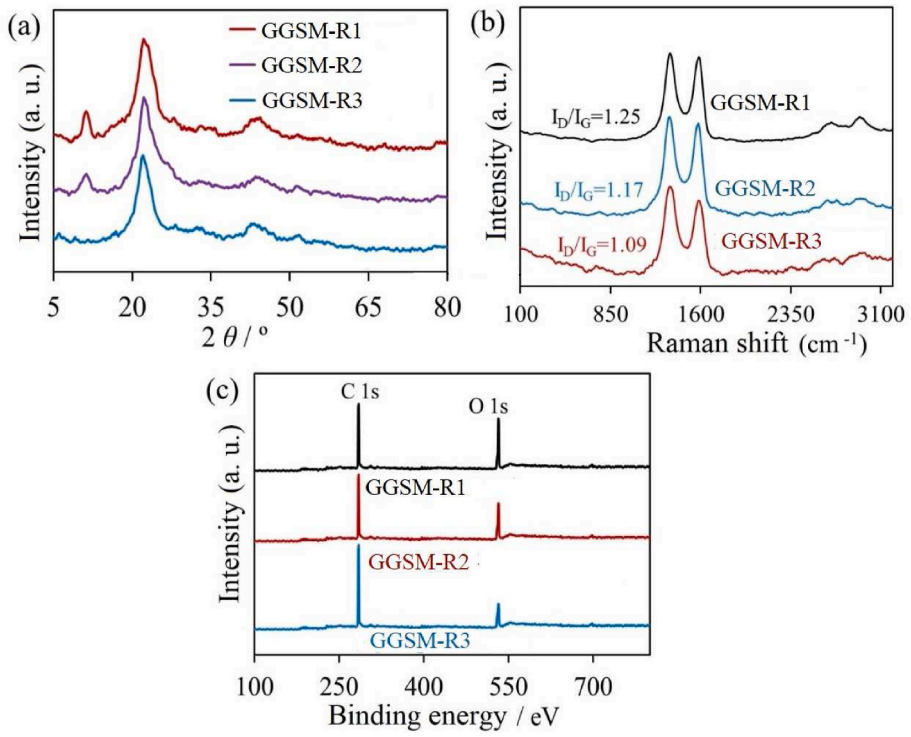

Fig. 8. (a) XRD, (b) Raman, and (c) XPS spectra of three different parts of the GGSM.

presence of three components: C in C–C/C═C bonds (285.4 eV), in C–*O*–C bonds (286.1 eV), in H–*O*–C═O bonds (296.0 eV) (figure S12a, c). O1s XPS spectrum of both materials showed peaks corresponding to C–O and C–OH bindings at about 531 and 532 eV (figure S12b and d) [33]. In fig. S12, the peak intensity of the oxygen-containing bonds in GGSM is much higher than those in GSM, suggesting the presence of considerable oxygenation parts of GGSM by the oxidation process.

fig. S13 shows N_2 adsorption-desorption isotherm and pore size distribution of GGSM-R3 and GGSM-R1. As seen in fig. S13, GGSM exhibited a typical hysteresis cycle and mesoporous pore structure [34,35]. The isotherm curves were fitted according to the BET model and the BET surface areas for different regions of the GGSM were presented in table S2. BET surface areas were calculated as 122 and 55 m^2/g for GGSM-R3 and GGSM-R1, respectively, indicating that the BET surface area decreases due to the deterioration of the pore structure with oxidation in the GGSM. In addition, the pore volume and average pore size of GGSM were determined according to the Barrett−Joyner−Halenda (BJH) method [36] (table S2). Both the pore volume and pore size decreased as the hydrophilic character increased in the GGSM structure.

3.5. The amount of water adsorption and swelling with water of GSM and GGSM

The rapid and effective absorption of water through the material is one of the parameters that affect the performance of solar steam generators. For this, the water transport rate for each material was first determined by monitoring the time-dependent movement of water. GSM and GGSM were prepared in a cylindrical shape (2 cm in length and 0.6 cm in diameter) and one side of each material was immersed in 4.0 mM Rhodamine B (Rh B) aqueous solution. The time-dependent movement of the Rh B solution for the sponge materials was monitored with a camera and recorded in Video S1 and Video S2, respectively. Compared to GGSM, GSM adsorbed Rh B solution rather slowly, which is due to the high hydrophobic character. Moreover, the solution absorption of GGSM was in a short time of about 10 s.

The weight swelling ratios (η_w, %) of GSM and GGSM were measured by immersing the pre-weighed dry samples in deionized water at various temperatures (20, 30, 40, and 50 °C) until equilibrium (fig. S14). After the materials were completely saturated with water, excess surface water was removed with filter paper, and fully swollen samples were weighed. η_w is calculated from the following equation [37];

$$\eta_W = \frac{m_s - m_d}{m_d} x100$$

where m_s is the weight of the swollen state of the sample at equilibrium and m_d is the weight of the dry state of the sample. The ηw values of GSM and GGSM obtained at different temperatures were presented in table S3.

Volume swelling ratios (η_V, %) of GSM and GGSM were determined by measuring sample size before and after swelling with water. η_V is calculated from the following equation;

$$\eta_V = \frac{V_s - V_d}{V_d} x100$$

where V_s is the volume of the swollen state of the sample at equilibrium and V_d is the volume of the dry state of the sample. The η_V values of GSM and GGSM at different temperatures are presented in table S4. As expected, GSM has very low η_w and η_V values compared to GGSM due to its high hydrophobic character.

As a result of the water absorption and water swelling experiments performed for each material, the water uptake rates of GSM and GGSM were calculated as 0.08 and 61.72 kg m^{-3} s^{-1}, respectively. Due to the hydrophobic structure, GSM absorbed very little water, whereas GGSM, possessing a hydrophilic structure displayed effective water absorption. The water carrying capacity of GGSM is higher than the steam generation rate under 1 sunlight, which is of great importance for the process to continue without slowing down, as rapid water absorption will prevent drying during the photothermal process.

3.6. Thermal conductivities of GSM and GGSM

The thermal conductivities of GSM and GGSM were measured by cutting the materials into about 2 x 2 × 2 cm dimensions and sandwiching them between two glass sheets, as dry and wet. The prepared "Sandwich" was placed between a hot (ceramic plate warmer) and a cold source (ice water bath). The temperature distribution along the cross-section of the sandwich structure was monitored using an IR camera. Thermal conductivity was determined using the Fourier equation;

$$q' = K\frac{dT}{dx}$$

where q' is the thermal conductivity per unit area, dT is the temperature difference, dx is the width of the sample and K is the thermal conductivity of the glass. The conductivity of the glass is 1.05 W m^{-1} K^{-1} (for 3 mm thickness of glass). The thermal conductivity calculation is based on the assumptions that the sample and glass slides are exposed to the same heat flux and the emissivity coefficients of the sample and the glass sheet are both 0.9 [25,38].

Since thermal insulation plays an important role in trapping heat on the evaporation surface during photothermal conversion, the thermal conductivity of GSM and GGSM was investigated in both wet and dry conditions. In the experimental study, the thermal conductivity was obtained by measuring the steady-state temperature difference for each material, where one side is heated and the other side is cooled. Thermal camera images of the dry and wet states of each material are presented in fig. S15. According to the thermal conductivity values (fig. S16) and the thermal conductivity values in wet and dry conditions (table S5), the materials have much lower thermal conductivity values (0.61 W m^{-1} K^{-1}) than that of water. Thus, it was determined that the water adsorbed by both GSM and GGSM could evaporate with lower energy and it was demonstrated that these materials could be applied in solar steam generators.

3.7. Solar steam generation applications of GSM and GGSM

The water evaporation rates for both GSM and GGSM were determined using the experimental setup in fig. S17. First, the system was used without the photothermal material. There is no obvious evaporation with no sunlight (Fig. 9, black dashed lines). When sunlight comes directly to the water surface, a certain level of evaporation is observed due to the heat energy of sunlight (Fig. 9, red dashed lines). There was a significant increase in steam generation performance for the system where both the sunlight was turned on and the prepared photothermal materials were used (Fig. 9, blue solid lines). Evaporation performances for GSM and GGSM after 1 h (Fig. 8) were calculated as 1.58 and 1.79 kg/m^2h, respectively. The low water transport rate of GSM is due to the lower evaporation rate of this material compared to GGSM.

fig. S18 shows the evaporation rate depending on the solar energy intensity for both GSM and GGSM. It can be seen that the evaporation rate increases proportionally as the solar energy intensity increases (fig. S18). Thus, the materials are sensitive to solar energy intensity and exhibit linear evaporation rates according to the solar energy intensity increment.

For the long-term stability of GSM and GGSM, evaporation rates were determined for 25 cycles using the same material under the same experimental conditions (figure S19a). In each cycle, wet-swelled material was removed from the system, and the material's adsorbed water was removed by applying a mass pressure. The material was dried at 60 °C for 20 min and reused in the next cycle. fig. S19 a displays the

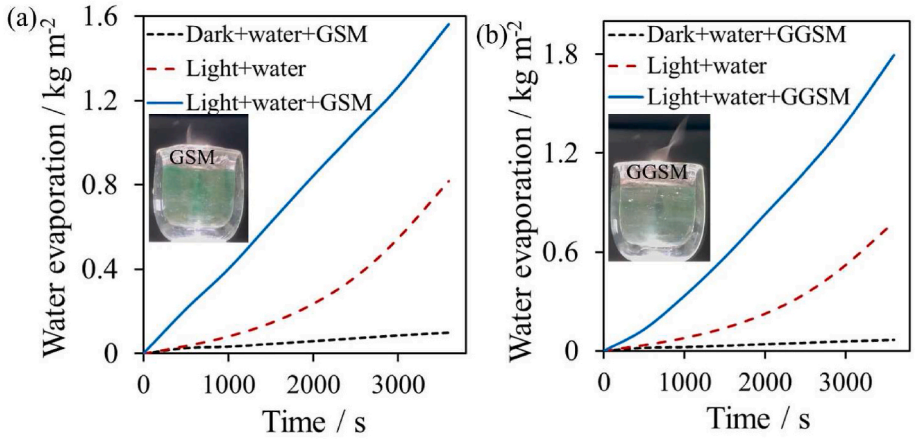

Fig. 9. The amount of water evaporation for (a) GSM, and (b) GGSM over time in the dark and under sunlight. Inset: The photographs of GSM and GGSM at the 40th under sunlight.

evaporation efficiency for GSM and GGSM and these materials maintained their initial value at 95% and 97% after the 10th cycle, and at 80% and 88% after the 25th cycle, respectively. The decrease in evaporation performance can be attributed to the structural deformation of graphene structures as a result of wetting and drying. As a result, both materials exhibited high cycle stability, which was attributed to the structural stability of graphene sponges.

To test the reproducibility, four GSMs and GGSMs were prepared with the same method and each was used as a photothermal converter in solar steam generators. fig. S19 b shows that GSMs and GGSMs exhibited close evaporation rates with relative errors of 0.5% and 0.3%, respectively, indicating owning high reproducibility of the materials.

The inset of Fig. 8, the GSM and GGSM photographs under sunlight at 40th trial demonstrated that the amount of vapor formed on the surface of the GGSM during the same period is higher than that of the GSM. Vapor generation performance of depending on GSM and GGSM irradiation time are presented in Video S3 and Video S4, respectively. In addition, the steam generation performance during the irradiation of the pure water surface at the same time without using any material is displayed in Video S5.Under optimum conditions for GSM and GGSM materials, temperature changes on their surfaces and in the system were recorded and monitored with a thermal camera during 100 s of irradiation (1 under sunlight, 1 kW m^{-2}) in. For GSM and GGSM, the surface temperatures after irradiation for a short period of 60 s were determined

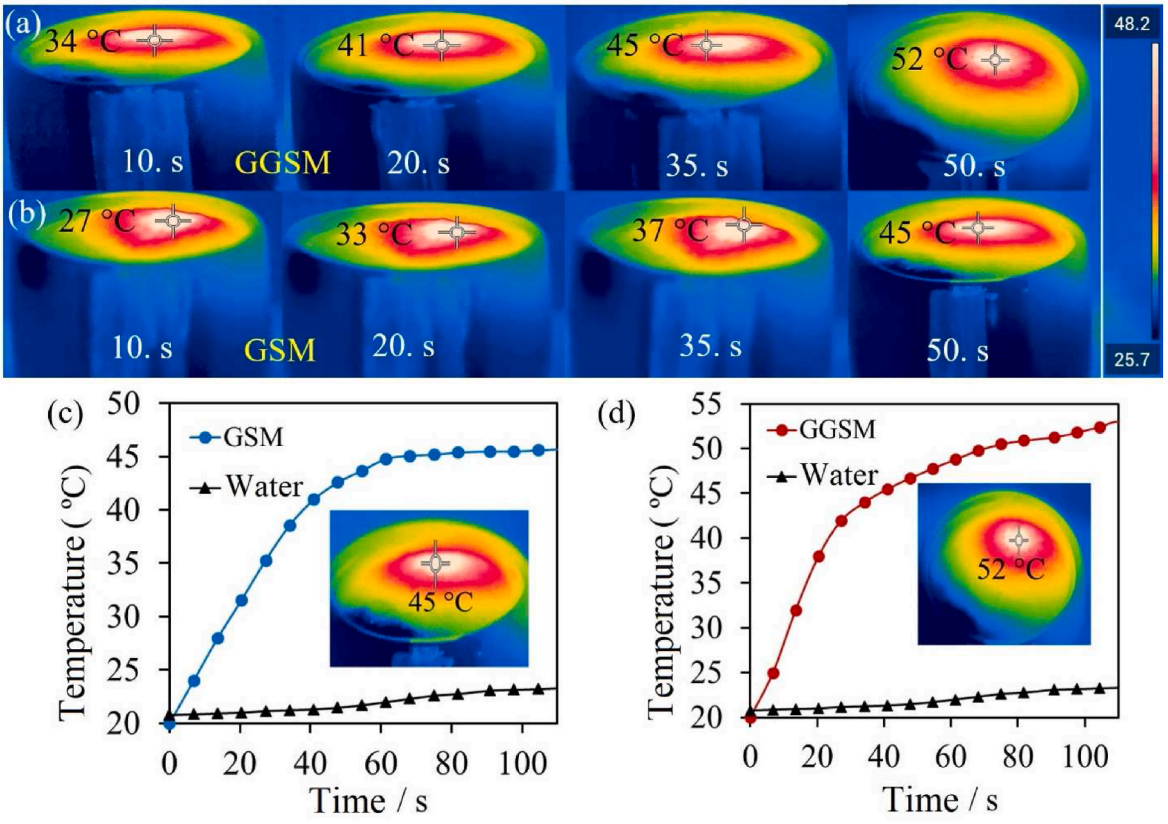

Fig. 10. Thermal camera images after different irradiation times for (a) GGSM and (b) GSM. Comparison of the temperature changes of (c) GSM and (d) GGSM to that of directly on the water surface during the 100 s irradiation for the system.

as 45 °C and 52 °C, respectively.

The change in surface temperature of the sponge materials, and the direct Fig. 10a and b water surface was investigated during 100 s irradiation time in Fig. 10c and d. These values are: for GSM from 20 to 45 °C, for GGSM from 20 to 52 °C, and for the direct water from 20 to 25 °C.The increase in surface temperature for GSM and GGSM was attributed to the photothermal activity of the graphene structure.

The solar thermal conversion efficiency (η) is expressed as:

$$\eta = \frac{mh_{LV}}{I}$$

where η is the solar vapor conversion efficiency, m is the evaporation rate, h_{LV} is the sum of the total enthalpy of sensible heat and the phase change enthalpy of the liquid, and I is the energy of sunlight [39].

The solar thermal conversion efficiency for GSM and GGSM was calculated as 45% and 57%, respectively. When GGSM and GSM are compared, it could be suggested that the thermal efficiency increases due to the gradient structure, and even the gradient structure contributes to the increase in the evaporation rate by reducing other heat losses.

The comparison of GGSM with various materials on SSG performance is presented in table S6. While most of the materials had a Janus structure possessing high thermal losses between the two layers, it was revealed that GGSM prepared in a uniform homogeneous structure had both high photothermal efficiency and high water absorption capacity. Furthermore, another advantage of our study is that GGSM is prepared with an easy-to-apply method compared to other Janus materials.

As a promising material for efficient solar steam generation, GGSM can steadily produce clean water from (Mediterranean and Black Sea) seawater. After distillation, about 99.9% and 99.8% desalination were achieved considering the Na^+ ions from the Mediterranean and Black Sea waters, respectively. In addition, it was observed that sea salt accumulated on the surface of the GGSM after desalination in the photograph of the GGSM (fig. S20). Meanwhile, the concentration of Na^+ ions is below the salinity levels defined by the World Health Organization (WHO). Our results demonstrate that GGSM is for the efficient utilization of solar energy for clean water, which is expected to be used for solar steam generation to solve the issue of cleaning water.

The steam generation efficiency of GGSM prepared in this work in solar steam generators is high compared to the materials prepared with graphene [9,17,40]. The efficiency can be further increased by the modification of graphene-based materials with substances absorbing sunlight effectively. Hence, modification of GGSM with new type supramolecules will be our future research plan for a more efficient, stable, and reusable steam generation approach.

4. Conclusion

In summary, 3D, flexible, light, and mechanically durable GGSM with hydrophobic character was prepared for solar steam generators. A simple acid impregnation method was used to prepare GGSM from hydrophobic GSM. Parameters such as acid type, acid composition, and acid treatment time are optimized for the preparation of this gradient sponge material. The structural and morphological characterizations with the analysis of hydrophilic and hydrophobic regions showed that GGSM has a gradient structure. Thanks to its partially hydrophilic region, the water uptake rate of GGSM is higher than that of GSM. Moreover, GGSM exhibited excellent solar steam generation performance (1.79 kg/m^{2}h) due to the higher water transport rate of the gradient structure compared to GSM (1.58 kg/m^{2}h). This study exhibited that the approach of the gradient structure of graphene sponge has great potential to develop high-performance materials for solar steam conversion.

CRediT authorship contribution statement

Elif Erçarıkcı: Investigation, Formal analysis, Data curation. **Ezgi Topçu:** Investigation, Formal analysis. **Züleyha Kudaş:** Investigation, Formal analysis. **Zeriş Aksu:** Investigation. **Murat Alanyalıoğlu:** Methodology. **Kader Dağcı Kıranşan:** Writing – review & editing, Writing – original draft, Validation, Resources, Methodology, Investigation, Funding acquisition, Formal analysis, Data curation.

Declaration of competing interest

The authors declare that they have no known competing financial interests or personal relationships that could have appeared to influence the work reported in this paper.

Data availability

Data will be made available on request.

Acknowledgments

This study was supported by the Scientific and Technological Research Council of Turkey (TUBITAK) under Project no. 121M347 and Atatürk University (Project: BAP-FDA-2022-10828).

Appendix A. Supplementary data

Supplementary data to this article can be found online at https://doi.org/10.1016/j.mtsust.2024.100701.

References

[1] K.S. Novoselov, D. Jiang, F. Schedin, T.J. Booth, V. V Khotkevich, S. V Morozov, A. K. Geim, Novoselov_Geim_PNAS_2005_2D atomic crystals.pdf 102 (2005) 10451–10453.
[2] E. Topçu, K. Dağcı Kıranşan, Electrochemical simultaneous sensing of melatonin and ascorbic acid at a novel flexible B-RGO composite paper electrode, Diam. Relat. Mater. 105 (2020) 107811, https://doi.org/10.1016/j.diamond.2020.107811.
[3] E. Ercarikci, K. Dagci Kiransan, E. Topcu, A flexible graphene paper electrochemical sensor with Electrodeposited Ag and Ni nanoparticles for H2O2Detection, IEEE Sens. J. 23 (2023) 7087–7094, https://doi.org/10.1109/JSEN.2023.3246380.
[4] E. Erçarıkcı, E. Topçu, K.D. Kıranşan, Flexible supercapacitor Electrodes based on modified binary metal phosphites on three dimensional graphene sponge, J. Alloys Compd. 930 (2022) 167305, https://doi.org/10.1016/j.jallcom.2022.167305.
[5] E. Erçarıkcı, E. Topçu, K. Dağcı Kıranşan, Three-dimensional FeNiP decorated graphene sponge: a novel flexible electrode for high-performance asymmetric supercapacitor, Mater. Res. Bull. 165 (2023), https://doi.org/10.1016/j.materresbull.2023.112333.
[6] T. Zeng, D. Feng, Q. Peng, Q. Liu, G. Xi, G. Chen, Nano-GeTe embedded in a three-dimensional carbon sponge for flexible Li-ion and Na-ion battery anodes, ACS Appl. Mater. Interfaces 13 (2021) 15178–15189, https://doi.org/10.1021/acsami.0c22616.
[7] X. Gu, Y. Deng, C. Wang, Fabrication of anion-exchange polymer layered graphene-melamine electrodes for membrane capacitive deionization, ACS Sustain. Chem. Eng. 5 (2017) 325–333, https://doi.org/10.1021/acssuschemeng.6b01685.
[8] K. Dağcl Klranşan, E. Topçu, Conducting polymer-reduced graphene oxide sponge electrode for electrochemical detection based on DNA hybridization, ACS Appl. Nano Mater. 3 (2020) 5449–5462, https://doi.org/10.1021/acsanm.0c00782.
[9] Y. Yang, R. Zhao, T. Zhang, K. Zhao, P. Xiao, Y. Ma, P.M. Ajayan, G. Shi, Y. Chen, Graphene-based standalone solar energy converter for water desalination and purification, ACS Nano 12 (2018) 829–835, https://doi.org/10.1021/acsnano.7b08196.
[10] M. Elimelech, W.A. Phillip, The future of seawater desalination: energy, technology, and the environment, Science 333 (2011) 712–717, https://doi.org/10.1126/science.1200488, 80-.
[11] L. Zhang, B. Tang, J. Wu, R. Li, P. Wang, Hydrophobic light-to-heat conversion membranes with self-healing ability for interfacial solar heating, Adv. Mater. 27 (2015) 4889–4894, https://doi.org/10.1002/adma.201502362.
[12] H.H. Richardson, Z.N. Hickman, A.C. Thomas, M.E. Kordesch, A.O. Govorov, Thermo-optical properties of nanoparticles and nanoparticle complexes embedded in ice: characterization of heat generation and actuation of larger-scale effects, Mater. Res. Soc. Symp. Proc. 964 (2006) 1–6, https://doi.org/10.1557/proc-0964-r03-18.
[13] K. Bae, G. Kang, S.K. Cho, W. Park, K. Kim, W.J. Padilla, Flexible thin-film black gold membranes with ultrabroadband plasmonic nanofocusing for efficient solar vapour generation, Nat. Commun. 6 (2015) 1–9, https://doi.org/10.1038/ncomms10103.

[14] L. Zhou, Y. Tan, J. Wang, W. Xu, Y. Yuan, W. Cai, S. Zhu, J. Zhu, 3D self-assembly of aluminium nanoparticles for plasmon-enhanced solar desalination, Nat. Photonics 10 (2016) 393–398, https://doi.org/10.1038/nphoton.2016.75.
[15] X. Li, W. Xu, M. Tang, L. Zhou, B. Zhu, S. Zhu, J. Zhu, Graphene oxide-based efficient and scalable solar desalination under one sun with a confined 2D water path, Proc. Natl. Acad. Sci. U.S.A. 113 (2016) 13953–13958, https://doi.org/10.1073/pnas.1613031113.
[16] Y. Li, T. Gao, Z. Yang, C. Chen, W. Luo, J. Song, E. Hitz, C. Jia, Y. Zhou, B. Liu, B. Yang, L. Hu, 3D-Printed, all-in-one evaporator for high-efficiency solar steam generation under 1 sun illumination, Adv. Mater. 29 (2017) 1–8, https://doi.org/10.1002/adma.201700981.
[17] P. Zhang, J. Li, L. Lv, Y. Zhao, L. Qu, Vertically aligned graphene sheets membrane for highly efficient solar thermal generation of clean water, ACS Nano 11 (2017) 5087–5093, https://doi.org/10.1021/acsnano.7b01965.
[18] X. Hu, W. Xu, L. Zhou, Y. Tan, Y. Wang, S. Zhu, J. Zhu, Tailoring graphene oxide-based aerogels for efficient solar steam generation under one sun, Adv. Mater. 29 (2017), https://doi.org/10.1002/adma.201604031.
[19] Z. Liu, H. Song, D. Ji, C. Li, A. Cheney, Y. Liu, N. Zhang, X. Zeng, B. Chen, J. Gao, Y. Li, X. Liu, D. Aga, S. Jiang, Z. Yu, Q. Gan, Extremely cost-effective and efficient solar vapor generation under nonconcentrated illumination using thermally isolated black paper, Glob. Challenges 1 (2017) 1600003, https://doi.org/10.1002/gch2.201600003.
[20] Y. Zeng, J. Yao, B.A. Horri, K. Wang, Y. Wu, D. Li, H. Wang, Solar evaporation enhancement using floating light-absorbing magnetic particles, Energy Environ. Sci. 4 (2011) 4074–4078, https://doi.org/10.1039/c1ee01532j.
[21] R. Niu, J. Ren, J.J. Koh, L. Chen, J. Gong, J. Qu, X. Xu, J. Azadmanjiri, J. Min, Bio-inspired sandwich-structured all-day-round solar evaporator for synergistic clean water and electricity generation, Adv. Energy Mater. 13 (2023) 1–10, https://doi.org/10.1002/aenm.202302451.
[22] N. Liu, L. Hao, B. Zhang, R. Niu, J. Gong, T. Tang, Rational design of high-performance bilayer solar evaporator by using waste polyester-derived porous carbon-coated wood, Energy Environ. Mater. 5 (2022) 617–626, https://doi.org/10.1002/eem2.12199.
[23] Z. Fan, J. Ren, H. Bai, P. He, L. Hao, N. Liu, B. Chen, R. Niu, J. Gong, Shape-controlled fabrication of MnO/C hybrid nanoparticle from waste polyester for solar evaporation and thermoelectricity generation, Chem. Eng. J. 451 (2022) 138534, https://doi.org/10.1016/j.cej.2022.138534.
[24] H. Ghasemi, G. Ni, A.M. Marconnet, J. Loomis, S. Yerci, N. Miljkovic, G. Chen, Solar steam generation by heat localization, Nat. Commun. 5 (2014) 1–7, https://doi.org/10.1038/ncomms5449.
[25] K.K. Liu, Q. Jiang, S. Tadepalli, R. Raliya, P. Biswas, R.R. Naik, S. Singamaneni, Wood-graphene oxide composite for highly efficient solar steam generation and desalination, ACS Appl. Mater. Interfaces 9 (2017) 7675–7681, https://doi.org/10.1021/acsami.7b01307.
[26] W.S. Hummers, R.E. Offeman, Preparation of graphitic oxide, J. Am. Chem. Soc. 80 (1958) 1339, https://doi.org/10.1021/ja01539a017.
[27] N.I. Kovtyukhova, P.J. Ollivier, B.R. Martin, T.E. Mallouk, E.V. Buzaneva, A. D. Gorchinskiy, Layer-by-layer assembly of ultrathin composite films from micron-sized graphite oxide sheets and polycations, Chem. Mater. 11 (1999) 771–778, https://doi.org/10.1021/cm981085u.
[28] E. Topçu, K. Dağcı, M. Alanyalıoğlu, Free-standing graphene/poly(methylene blue)/AgNPs composite paper for electrochemical sensing of NADH, Electroanalysis 28 (2016) 2058–2069, https://doi.org/10.1002/elan.201600108.
[29] E. Erçarlkcl, K. Dağcl Klranşan, E. Topçu, Three-dimensional ZnCo-mof modified graphene sponge: flexible electrode material for symmetric supercapacitor, Energy Fuel. 36 (2022) 1735–1745, https://doi.org/10.1021/acs.energyfuels.1c04183.
[30] M.W. Khan, J. Yao, K. Zhang, X. Zuo, Q. Yang, H. Tang, K.M.U. Rehman, H. Zhang, G. Li, S. Jin, M. Wu, Engineering N-reduced graphene oxide wrapped Co3O4@f-MWCNT hybrid for enhance performance dye-sensitized solar cells, J. Electroanal. Chem. 844 (2019) 142–154, https://doi.org/10.1016/j.jelechem.2019.05.008.
[31] S.S. Patil, M.A. Johar, M.A. Hassan, D.R. Patil, S.W. Ryu, Enhanced photoelectrocatalytic water oxidation using CoPi modified GaN/MWCNTs composite photoanodes, Sol. Energy 178 (2019) 125–132, https://doi.org/10.1016/j.solener.2018.12.028.
[32] D. Nath, R. Das, Experimental (XRD) and theoretical (DFT) analysis for understanding the influence of SHI irradiation on the stacking fault energy in CdSe nanocrystals, J. Alloys Compd. 879 (2021), https://doi.org/10.1016/j.jallcom.2021.160456.
[33] G. Wang, L. Zhang, J. Zhang, A review of electrode materials for electrochemical supercapacitors, Chem. Soc. Rev. 41 (2012) 797–828, https://doi.org/10.1039/c1cs15060j.
[34] J. Luo, J. Lai, N. Zhang, Y. Liu, R. Liu, X. Liu, Tannic acid induced self-assembly of three-dimensional graphene with good adsorption and antibacterial properties, ACS Sustain. Chem. Eng. 4 (2016) 1404–1413, https://doi.org/10.1021/acssuschemeng.5b01407.
[35] Y. Li, H. Bin Zhang, L. Zhang, B. Shen, W. Zhai, Z.Z. Yu, W. Zheng, One-pot sintering strategy for efficient fabrication of high-performance and multifunctional graphene foams, ACS Appl. Mater. Interfaces 9 (2017) 13323–13330, https://doi.org/10.1021/acsami.7b02408.
[36] J. Sha, C. Gao, S.K. Lee, Y. Li, N. Zhao, J.M. Tour, Preparation of three-dimensional graphene foams using powder metallurgy templates, ACS Nano 10 (2016) 1411–1416, https://doi.org/10.1021/acsnano.5b06857.
[37] X. Yin, Y. Zhang, Q. Guo, X. Cai, J. Xiao, Z. Ding, J. Yang, Macroporous double-network hydrogel for high-efficiency solar steam generation under 1 sun illumination, ACS Appl. Mater. Interfaces 10 (2018) 10998–11007, https://doi.org/10.1021/acsami.8b01629.
[38] Y. Xu, J. Wang, F. Yu, Z. Guo, H. Cheng, J. Yin, L. Yan, X. Wang, Flexible and efficient solar thermal generators based on polypyrrole coated natural latex foam for multimedia purification, ACS Sustain. Chem. Eng. 8 (2020) 12053–12062, https://doi.org/10.1021/acssuschemeng.0c03164.
[39] C. Kim, D. Shin, M.N. Baitha, Y. Ryu, A.M. Urbas, W. Park, K. Kim, High-efficiency solar vapor generation boosted by a solar-induced updraft with biomimetic 3D structures, ACS Appl. Mater. Interfaces 13 (2021) 29602–29611, https://doi.org/10.1021/acsami.1c05883.
[40] X. Wang, G. Ou, N. Wang, H. Wu, Graphene-based recyclable photo-absorbers for high-efficiency seawater desalination, ACS Appl. Mater. Interfaces 8 (2016) 9194–9199, https://doi.org/10.1021/acsami.6b02071.